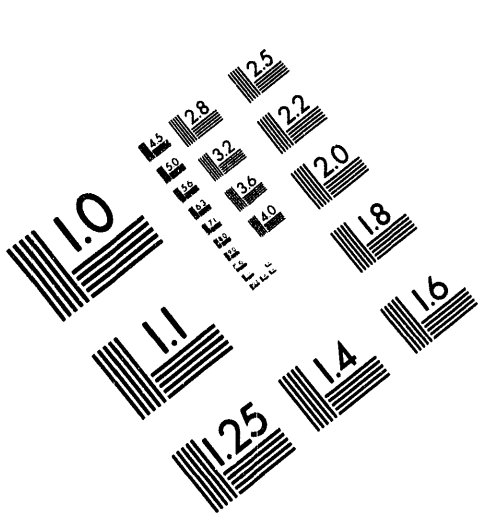

Association for Information and Image Management
1100 Wayne Avenue, Suite 1100
Silver Spring, Maryland 20910
301/587-8202

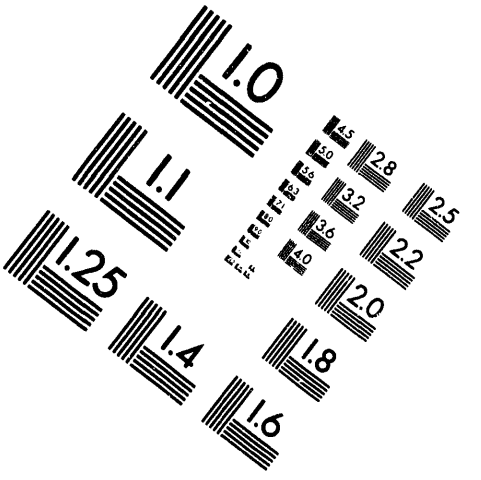

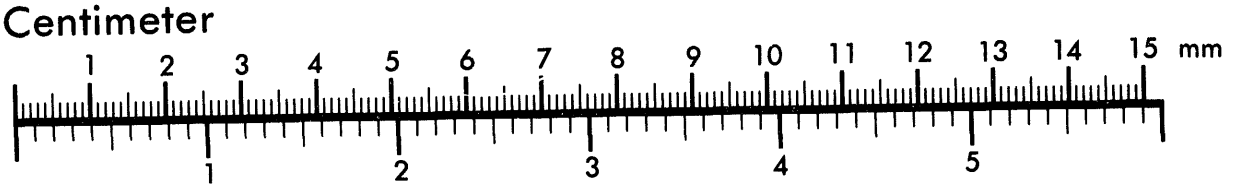

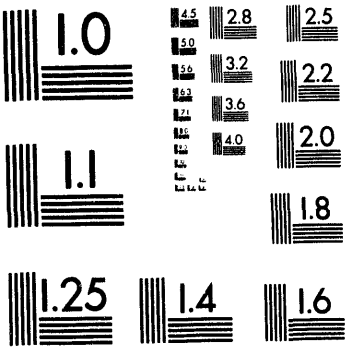

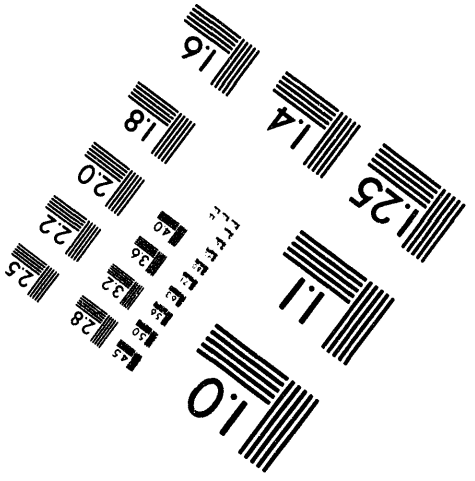

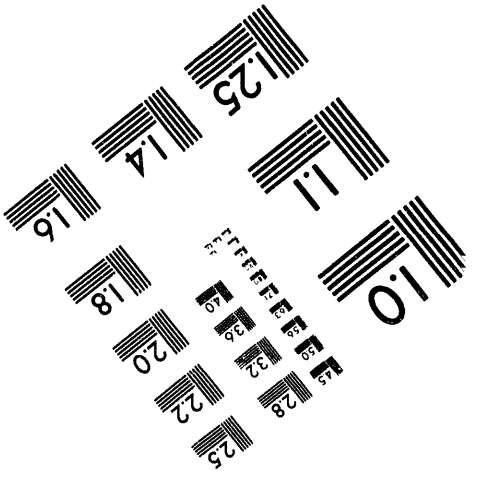

MANUFACTURED TO AIIM STANDARDS
BY APPLIED IMAGE, INC.

1 of 1

Conf-9309103--8

UCRL- JC-113387
PREPRINT

CALCULATIONS OF THE FLAX EVENTS WITH COMPARISONS TO PARTICLE VELOCITY DATA RECORDED AT LOW STRESS

J. Rambo, LLNL

Presented at the 7th Symposium on the Containment of Underground Nuclear Explosions,
Kent, WA
September 13-17, 1993

September, 1993

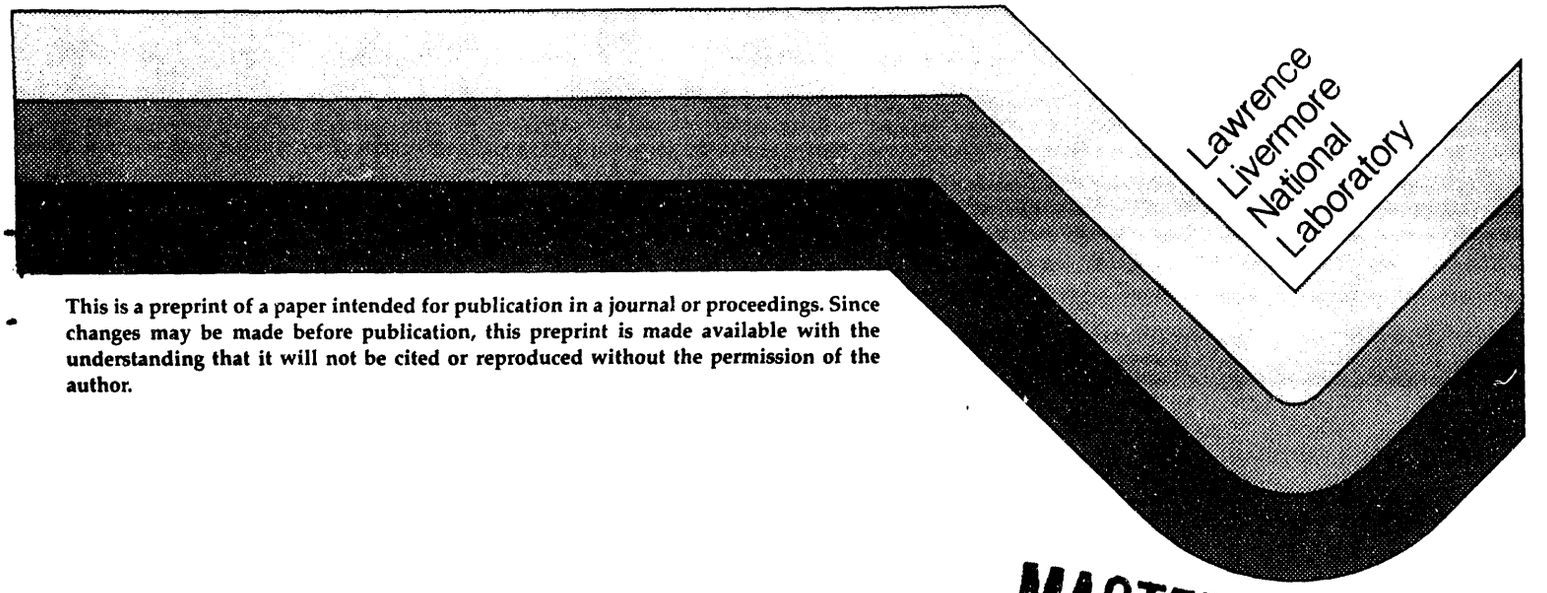

DISCLAIMER

Calculations of The FLAX Events with Comparisons to Particle Velocity Data Recorded at Low Stress

John Rambo, Lawrence Livermore National Laboratory

ABSTRACT

The FLAX event, fired in 1972, produced two particle velocity data sets from two devices in the same hole, U2dj. The data are of interest because they contain verification of focusing of a shock wave above the water table. The FLAX data show the peak velocity attenuation from the device buried in saturated tuff are different from those emanating from the upper device buried in porous alluvium. The attenuations of the peaks are different in regions traversed by both waves traveling at the same sound speed and measured by the same particle velocity gages. The attenuation rate from the lower device is due to 2-D effects attributed to wave focusing above the water table and is a feature that should be captured by 2-D calculations. LLNL's KDYNA[1] calculations used for containment analyses have utilized a material model initially developed by Butkovich, which estimates strength and compressibility based on gas porosity, total porosity, and water content determined from geophysical measurements. Unfortunately, the material model estimates do not correctly model the more important details of strength and compressibility used for matching the velocity data. The velocity gage data contain information that can be related to the strength properties of the medium, provided that there are more than two gages recording in the stress region of plastic deformation of the material. A modification to Butkovich's model incorporated approximate strengths derived from the data. The mechanisms of focusing will be discussed and will incorporate additional information from the TYBO event.

INTRODUCTION

Calculations used for containment analyses utilize a material model initially developed by Butkovich[2], which estimates strength and compressibility based on gas porosity, total porosity, and water content determined from geophysical measurements. We used this model to simulate ground motion for two nuclear detonations (the FLAX event) conducted in the same drill hole and separated in time by an amount that was sufficient to record separate ground motion features.

For the FLAX devices, the peak particle velocity attenuations are different in regions traversed by both elastic waves and measured by the same

*Work performed under the auspices of the U. S. Department of Energy by the Lawrence Livermore National Laboratory under contract number W-7405-ENG-48.

particle velocity gages. The wave propagation from the lower device is enhanced by the water saturation and by effects attributed to wave focusing above the water table. These are features that should be and are simulated by 2-D calculations. The velocity gage data contain information independent of yield that can be related to the strength properties of the medium provided that there are more than two gages recording in the stress region of plastic deformation of the material. A modification to Butkovich's model incorporated approximate strengths derived from such data. The strength modifications result in a better matching of the particle velocity data than using the default strengths from Butkovich's model.

FLAX PARTICLE VELOCITY OBSERVATIONS

The FLAX peak free surface velocities were unusual. FLAX was composed of two devices. The lower event with depth-of-burial, DOB, of 689 m was detonated about 30 s before the upper event with DOB of 435 m. The upper event which was about 3 times the yield of the lower device and closer to the surface gave a lower peak surface velocity (1.01 m/s) than the lower placed event (1.43 m/s). Figure 1 shows a symbolic representation of the relationship.

Limited data were available for analysis of this event. There were few velocity gages and some areas of the satellite hole had no coverage[3,4] as shown in Figure 2. However, the available gages revealed important phenomena. The gages above the upper device recorded velocities from both events and the attenuations of the peak velocities were measured through the same medium. Geophysical logs (1972)[5] were crude by todays standards. Review of recent events near the FLAX site, U2dj, show consistently higher grain density measurements[6,7]. The methodology for this measurement has improved over the years, and L. McKague[8] has suggested using measured grain density values from one of the nearby recent events. Some strength and compressibility measurements on cores were performed for only a few locations[9]. They did not provide a complete representation of the geology and were not used in this analysis.

Time-of-arrival (TOA) of the outgoing waves are useful to evaluate material crushing caused by the lower event that could change the material properties for the upper event. Where the peak of the particle velocity is propagating at near the sound speed, we assume that elastic or almost elastic behavior is in effect and either purely elastic compression or minimal crush and/or damage to the material is occurring. The elastic onset (the time of the first positive detectable particle velocity) and the following time of the peak particle velocity arrival are shown for each event in Figure 3.

The slopes of the TOA values in Figure 3 translate to velocity of the wave between points. The onset velocities represent the elastic sound speed of the material between the measurement points. The slope of the peaks can be compared to the slope of the elastic onset to determine where the peaks are undergoing large amounts of plastic failure. Above the standing water level (SWL) where the gas porosity is high, the lower event peak velocities travel slowly indicating plastic failure. Further above the SWL the peak abruptly increases to a sound speed similar to the speed of the elastic onset. Some minor time spread of the two parts of the wave occurs upward to a location just below the upper device. Above the upper working point the onset and peak travel parallel (the same sound speed) until just below the surface where spall obscures the timing of the peak. The fact of the same sound speed for both onset and peak velocity indicates very little crush up of the material has occurred above the upper device. The peak wave velocity from the upper device shows a similar slow velocity for the pore-crush followed by a higher sound speed velocity to the surface. The onsets and peaks from both devices travel with about the same sound speed through the same upper region of the FLAX site.

Attenuation of the peak particle velocity is material dependant. The most important factors are usually gas porosity and strength, where the peak of the wave is undergoing plastic failure. Where the wave is truly elastic, the attenuation should be R^{-1}. Particle velocity attenuations from calculations usually show an abrupt change in attenuation to R^{-1} when the stress falls below plastic failure into the elastic regime. This is accompanied by a sudden change to elastic sound speed at the same location. However, the data for the quasi-elastic attenuations do not follow the calculations in quite the same way.

A comparison of peak velocity vs range for both devices is shown in Figure 4. The range axis of the log-log plots is referenced to the depth-of-burial, DOB, of each device and the attenuation is determined from a power fit to the data, $Up=aR^b$, where b is the attenuation exponent and Up is the peak particle velocity. The upper event attenuation, b, is about -2.9 and uses three data points above 9 m/s and one point almost in the spall zone (0.7 m/s). There is no information on the attenuation between 0.7 and 9 m/s. However, the attenuation of -2.9 compares well with a more recent nearby event, CORNUCOPIA in hole U2gaS, with the value[10] of -3.2. The upper FLAX particle velocity values above 9 m/s were scaled to the particle velocities of CORNUCOPIA and resulted in a yield estimate very near the official yield.

INTERPRETATION OF THE FLAX DATA

From the scaling and the similarity in attenuations, the upper FLAX data are interpreted as "normal" for an alluvium event and the material was not significantly changed by the lower device. The porous alluvial events experience strong energy attenuation because of the material failure and PdV work that accompany pore-crush. This dissipates the wave's kinetic energy in the source region, and this decoupling is observed at seismic distances as well.

The lower device data show some unusual attenuations. Data from both devices have about the same particle velocity value at about 110 m range. Velocity (as a function of range) from the upper device attenuates steeply in porous material at a higher yield while the lower device velocities attenuate less steeply in a saturated material at a lower yield to get to about the same particle velocity at 110 m range. Above the 110 m range, the lower device data attenuation exponent is about -9.0 due to the gas porosity above the water table. The attenuation changes to -1.4 at about the place where sound speeds occur for the peak. An interesting observation is that the attenuations in the regions traversed at similar sound speeds are different for both peak velocity data sets as shown by the thickened lines of Figure 4. Since the upper data are normal and the material was not significantly changed by the lower event, then the lower device attenuation of -1.4 appears unusual. The objective was to understand this unusual attenuation.

MODEL

A material model which was first developed by Butkovich, estimates compressibility based on density, water content, grain density, Poisson's ratio, and longitudinal velocity. Strength in terms of the compressive elastic limit is estimated, and the user can estimate shear strength from the compressive elastic limit and Poisson's ratio if uniaxial strain is assumed. Additionally, strength can be estimated from particle velocity data where gage records are relatively close together and the peak velocities indicate plastic failure. Fortunately, both FLAX device data sets show plastic failure.

The calculational model consisted of several horizontal layers designed to capture some of the nuances of elastic properties and the gas porosity. Figure 5 shows some of the logging data that were the source of material properties used in the model. The trace of the density, longitudinal velocity

(DHAL)*, acoustic impedance, and wt% of H_2O are shown next to the rock type. The units are mixed between English and SI because the original logs are in English units from an unpublished document[11]. The depths of the layers are given in meters and the working points are shown in the left margin. The calculated value of gas porosity was derived from density (U2dj)[5], wt% H_2O (U2dj, UE2dj, U2ge), and grain density (U2ge)[6]. The most significant modeling of gas porosity was the water table interface at 574 m depth. Above the interface the gas porosity is 13 vol% and it has a large influence on the wave attenuation. The default elastic limit strengths from Butkovich's model are shown, as well as the modified strengths derived from the particle velocity data. The modified strengths are considerably weaker than the default values and were used only in the layers for which the strengths could be estimated from the data.

MODIFICATIONS TO DEFAULT STRENGTHS

The modified strength and compressibility relationship near the linear elastic region was modified from the default values of the Butkovich model values. Figure 6 shows schematically some of the process to refine the model. Two adjacent particle-velocity waveforms located above the water table were compared. The average elastic limit is selected based on the observance of a constant time difference between equivalent parts of the wave. Constant difference suggests those parts to be traveling at the same sound speed and are considered to be linear elastic in the model. Above this point equivalent parts of the wave spread in time as they represent higher pressures subjected to the porous crush-up of the material. The radial stress (σ_r) can be estimated from the highest particle velocity of constant time difference (U_p), the sound speed (U_s) calculated from the gage separation distance divided by the time separation, and the initial state density (ρ_0) by the conservation of mass equation for the jump condition, $\sigma_r = \rho_0 . U_s . U_p$. Assuming a Poisson ratio, the mean elastic pressure (P_m) and strength (τ) can also be estimated from the formulas shown in Figure 6, assuming the condition of uniaxial strain.

Above the elastic limit a qualitative picture of the shape of the P vs mu relationship was estimated from the incremental application of the conservation of mass formula. Since the velocities (Us) over the interval between the estimated elastic limit and the peak were increasingly slower, this equation was not quite appropriate, but more useful to give the approximate curvature in the low pressure regime than the default. Figure 6 shows a comparison with the default higher strength P vs mu

---

* Dry Hole Acoustic Log

compressional relationship compared to the derived lower strength relationship that is suggested from data. For the material just above the water table the two P vs mu curves tended to merge at higher pressures.

The P vs mu relationships below and above the water table are shown in Figure 7. This shows a large increase in compressibility that occurs across the water table at this site. The sound speed is related to the slope of the P vs mu relationship. As the pressure wave crosses the water table the velocity slows considerably as the wave travels into the more porous material.

AGREEMENT OF CALCULATED PEAK SURFACE VELOCITY TO DATA

Using the actual FLAX yields the agreement between calculations and the peak free surface velocity data from both devices was good. The tables in Figure 8 show the agreement. However, considering the simplicity and approximations of the model, the very close agreement was fortuitous. The upper device data did not model the near surface spall region very well and wave forms in this region were not well matched. The data from the lower device showed much better agreement with wave forms.

FOCUSING ABOVE THE WATER TABLE

The calculations were useful for explaining the high surface velocity from the lower FLAX device. Shock waves usually travel slow in porous material and more rapidly in the saturated material, for plastic stresses less than 500-MPa. The slope of the compressibility relationship, P vs mu, is quite different for saturated and porous alluvium for the pressure ranges occurring near the water table. The shock wave travels at high velocity and low attenuation up to the water table interface and with slow velocity and high attenuation above. The effect of slowing down can be seen in velocity contours of Figure 9. A circular contour line has been plotted over the second contour line to emphasize the shape difference below and above the water table (SWL). The wave is generally spherical in the calculation relative to the center of the explosion below SWL and has flattened considerably above.

The wave above the SWL is spherical as well but relative to a geometric center below the actual center as depicted schematically in Figure 10a. This is partially due to a Snell's Law effect at the SWL and has the analogy of focusing of light by a lens. The spherical divergence changes above the SWL as shown schematically with the solid radial lines from both geometric sources. Both 1-D and 2-D calculations have been compared using the same model parameters. The 1-D[12] calculations produce a spherical interface which eliminates the Snell's Law effect on the

calculation. The attenuation effect of divergence above the SWL is shown in the schematic comparison of Figure 10b. The 2-D calculation agrees well with the 1-D calculation radially to the SWL. Above the SWL the 2-D calculation shows higher velocities and lower attenuations.

AXIAL PREFERENCE OF PORE COLLAPSE FLATTENS THE WAVE FRONT

There is a second effect that contributes to focusing. The path between the lower device and the water table is shortest in the axial (vertical) direction. The stress at the water table is greatest at that point and diminishes horizontally along the water table as the wave takes longer paths (with more attenuation) to arrive. The highest stress, axial path at the SWL takes the longest porous crush-up time and distance to attenuate to elastic stress above the water table. The other paths take less crush up time and distance as shown in Figure 11. The crush up distance between the SWL and the curved line representing the location of elastic stress diminishes with horizontal distance. The decreasing time in the crush up has been observed from surface gages on the TYBO event[13]. The particle velocity vs time from locations along the ground surface showed greatest time separation between the elastic portion of the wave and the remnant of the plastic peak at surface ground zero (SGZ). Other observations on TYBO were very high SGZ surface velocity and a pronounced reduction of the peak surface velocities with horizontal distance.

SUMMARY

The surface velocities from both FLAX devices at first appeared anomalous. Comparisons with nearby alluvium event data indicate the upper FLAX device is a "normal" alluvium event and the velocity peak attenuation is similar. The sound speeds indicate that the alluvial material was not significantly changed by the passage of the stress wave from the lower FLAX device prior to the detonation of the upper event. The lower FLAX event has high peak surface velocity because of lower peak attenuation in the saturated medium below the water table and the 2-D effect of wave focusing above the water table. The focussing is attributed to two effects; Snell's Law and the preference of the shock to run slowly for a longer time during the pore-crush in the axial direction.

Significant improvements to the default FLAX modeling were due to well placed velocity gages from which strengths could be estimated. Further improvements for the FLAX modeling are possible, but most involve model changes based on the calculator's experience and are not easily justified without core measurements. There are measured strength data from core at some FLAX locations which could be incorporated in simulations. This

might resolve the issue of the importance of core samples. Other models developed for nearby events could be employed (such as a damage model)[14] to examine their sensitivity.

Improvements in the general process for a new event would require more velocity gages coupled with simulations to further develop material models. Perhaps analysis of Lagrangian measurements[15] (multiple velocity gages) could be employed to obtain better in-situ material properties. Core measurements at appropriate locations which include strength and compressibility would also be valuable.

ACKNOWLEDGEMENTS

I wish to thank J. White for reviewing the paper and for general technical discussions. Discussions about the wave propagation above the water table were very useful. I also thank Ted Butkovich for his help with the computer calculations and post processing, and C. Olsen for reviewing the paper.

REFERENCES

1. Levatin, J. L., Attia, A. V., and Hallquist, J. O., "KDYNA USER'S MANUAL", Lawrence Livermore National Laboratory, Livermore, CA, UCRL-ID-106104, 1990.
2. Butkovich, T. R., "A Technique for Generation Pressure-Volume Relationships and Failure Envelopes for Rocks", Lawrence Livermore National Laboratory, Livermore, CA, UCRL-51441, Nov., 1973.
3. Wheeler, V. E., Lawrence Livermore National Laboratory, private communication, May, 1973.
4. Preston, R. G., Lawrence Livermore National Laboratory, private communication, May, 1973.
5. LLN-N Geology, "Geology of Emplacement Hole U2dj (FLAX)", Lawrence Livermore National Laboratory internal memorandum, GN-6-72, April, 28, 1972
6. Clarke, S. R., and McKague, L., "U2ge Site Characteristics Summary", CP 87-36, April, 1987
7. Howard, N., "U2fa Preliminary Site Characteristics Summary", AGTG 77-39, April 29, 1977
8. McKague, L., Lawrence Livermore National Laboratory, 1992, private communication, (Currently with Southwest Research Institute, San Antonio, Texas)

9. Brandt, H., and Chu, H., "Triaxial Tests of Alluvium, Final Report", University of California Department of Mechanical Engineering, Davis California, Contract Order Number 2100603, 1977

10. Hudson, B., Lawrence Livermore National Laboratory, private communication, Sept., 1992.

11. Ramspott, L., "U2dj Site Characteristics Report", Lawrence Livermore National Laboratory, Internal Memorandum, Unpublished, March 30, 1972

12. Snell, C. M. and Austin, M. G., "SOC Code: Lagrangian, Finite-Difference Calculational Technique in One-Dimensional Symmetry", Lawrence Livermore National Laboratory, Livermore, CA, UCID-18220, July, 1979.

13. Rambo, J. T., and Bryan, J. B., "Calculation of High Surface Velocity Due to Focusing in the TYBO Event", Proceeding of the Second Containment Symposium, Kirkland AFB, Albuquerque, NM, August 2-4, 1983.

14. N. Rimer, and W. Proffer, "Containment Phenomenology Using a New Shear-Strain-Based Computational Model for Tuff", 6th Symposium on Containment of Underground Nuclear Explosions, CONF-9109114-VOL1, Lawlor Events Center, University of Nevada, Reno, Nevada, September 24-27, 1991.

15. Aidun, J. B., and Gupta, Y. M., "Analysis of Lagrangian Gauge Measurements of Simple and Nonsimple Plane Waves", J. Appl. Phys. 69 (10), May 15, 1991.

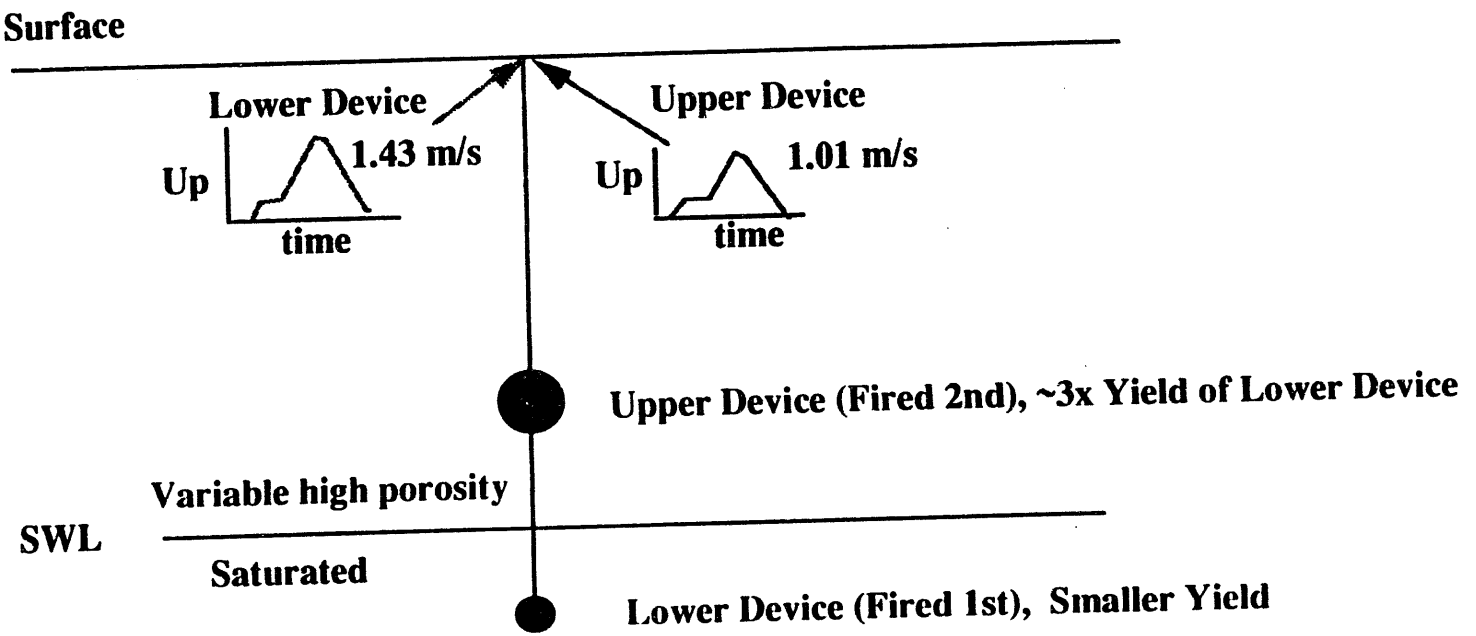

Figure 1. Schematic of device position and particle velocity results. Lower device is buried below the standing water level (SWL) and gives a higher peak surface velocity than the shallower, larger yield event.

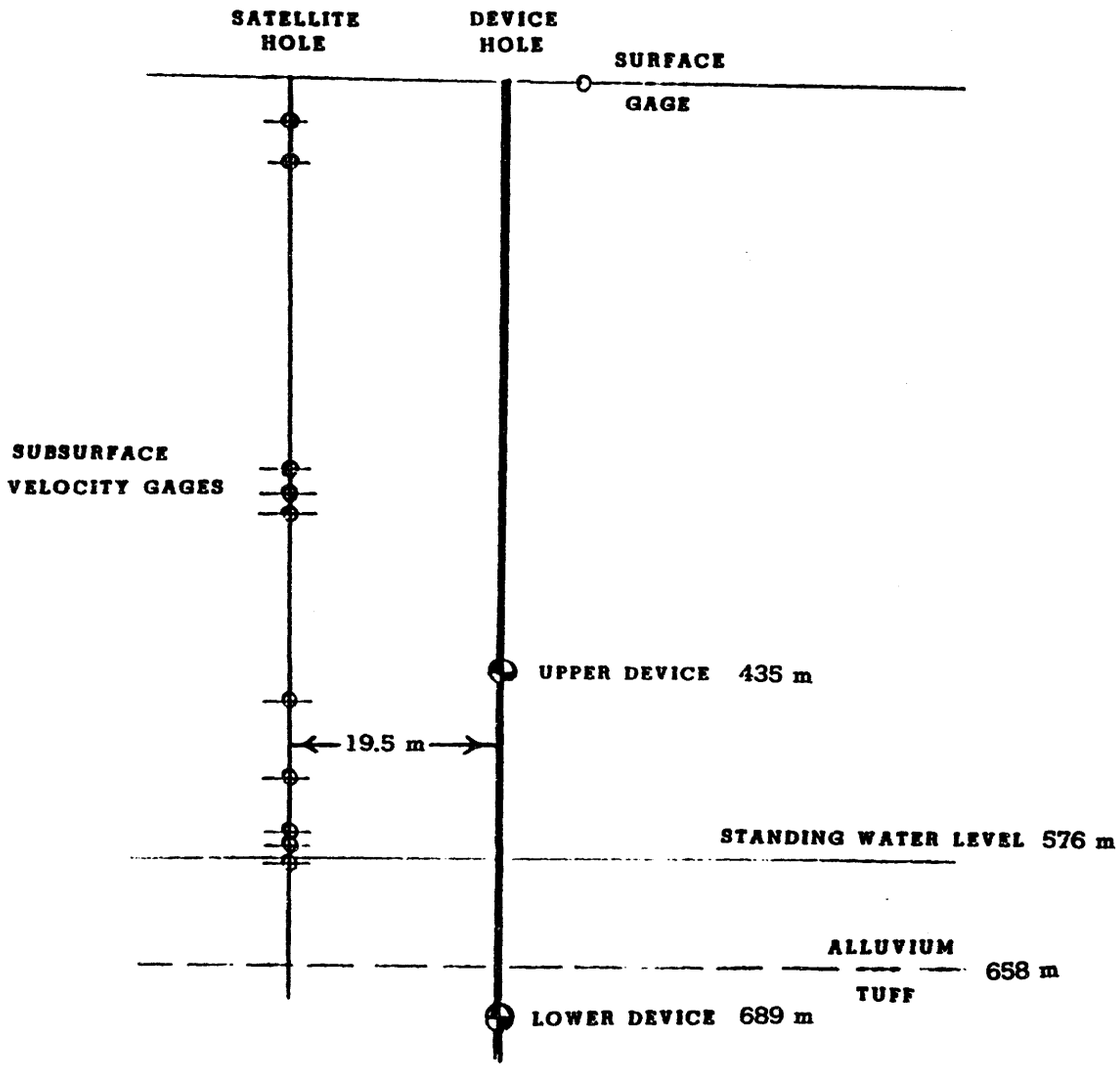

Figure 2. Schematic of gage locations relative to device locations. Gages above upper device recorded data from both devices.

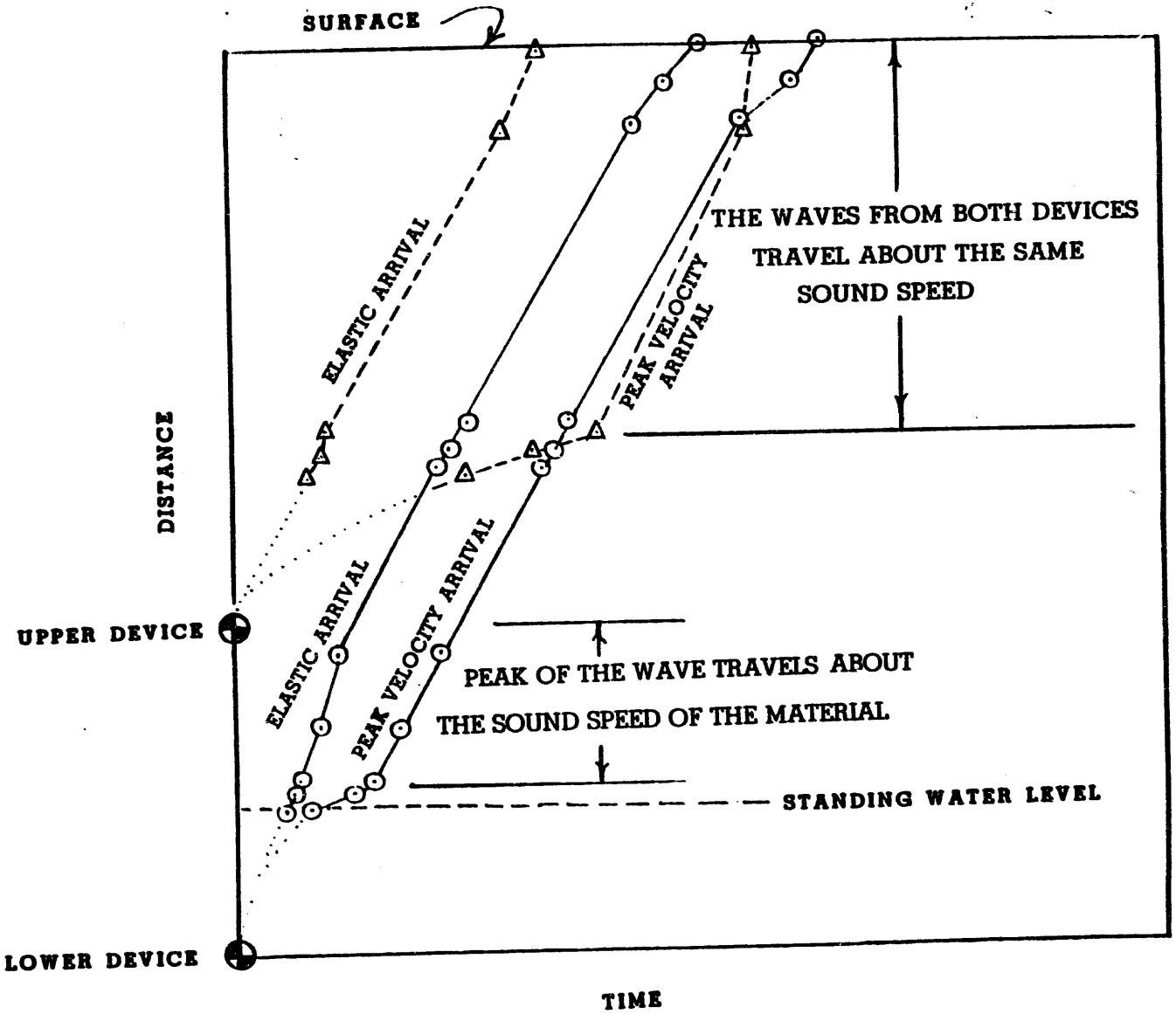

Figure 3. Time-of-arrival of elastic onset and the peak of the velocity wave from both devices. The peak velocity wave from the lower device (solid lines) travels at the sound speed before it passes the upper device. The peak particle velocity wave from the upper device (dashed lines) travels at about the same sound speed as does the lower one.

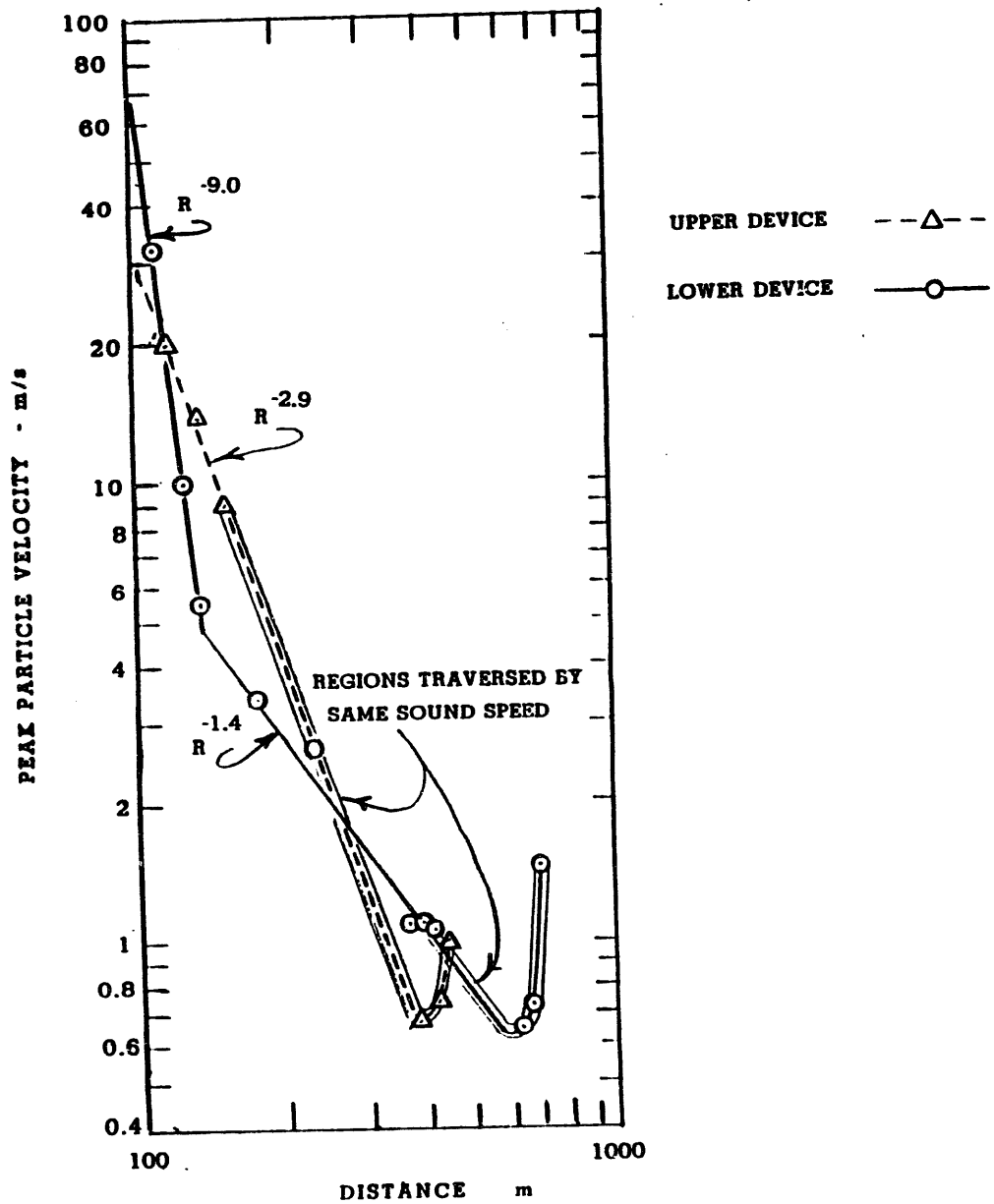

Figure 4. Peak particle velocity vs attenuation from both devices. Thick lines are areas traversed by waves from both devices at the same sound speed but both have different attenuation exponents.

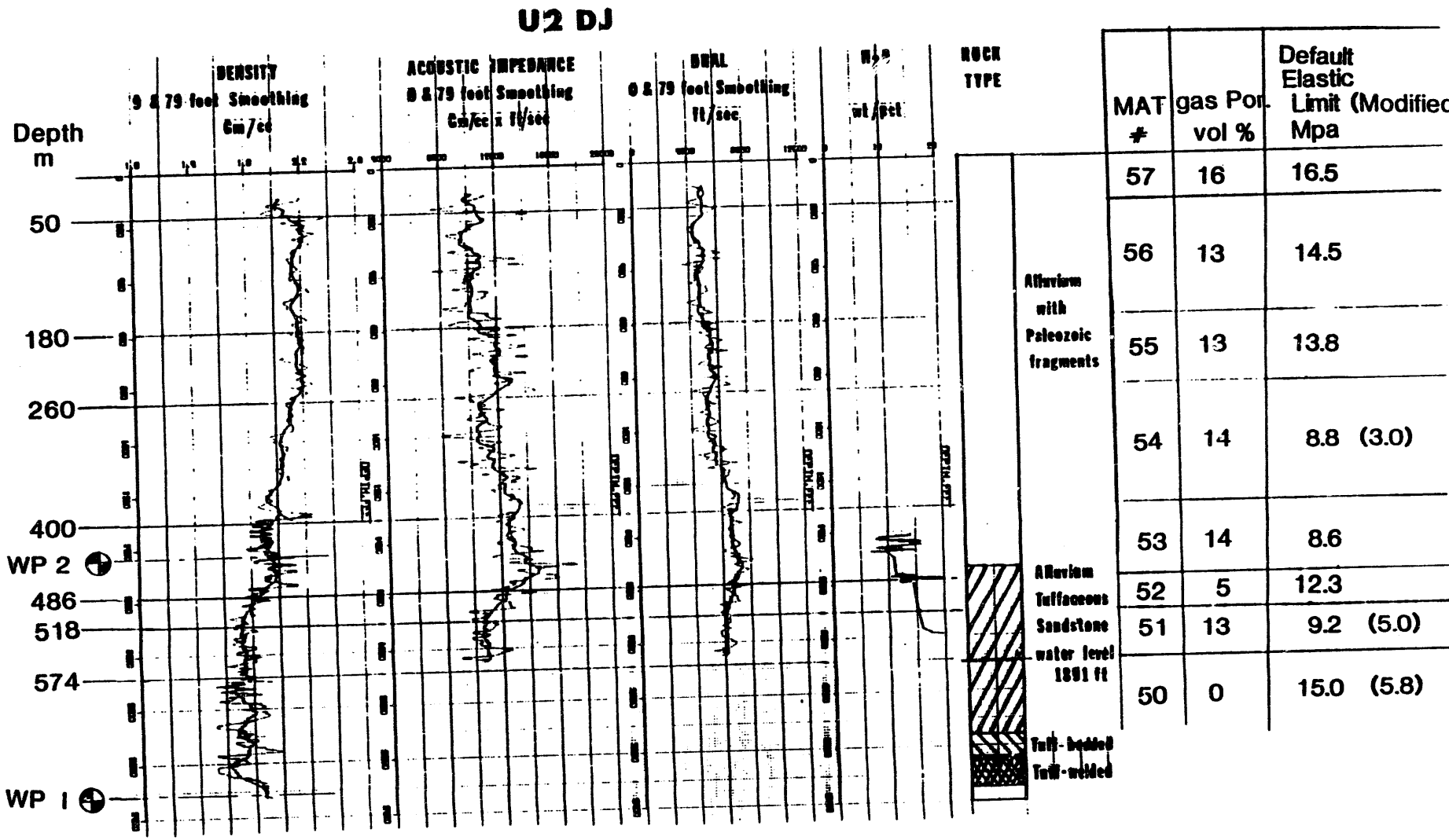

MAT #	gas Por. vol %	Default Elastic Limit (Modified) Mpa
57	16	16.5
56	13	14.5
55	13	13.8
54	14	8.8 (3.0)
53	14	8.6
52	5	12.3
51	13	9.2 (5.0)
50	0	15.0 (5.8)

Figure 5. Geophysical model showing geophysical logs, selected layers, gas porosity, rock type and strength. Modified strengths are shown in parentheses. Gas porosity above water table (574 m depth) and strengths are the most important aspects of the model.

Estimation of the elastic limit

For the elastic case

$\sigma_r = \rho_o \cdot U_s \cdot U_p$

Assuming uniaxial strain and a

Poisson's ratio, ν, mean stress, P_m,

and shear strength, τ, can be estimated.

$$P_m = \frac{\sigma_r}{3}\left[\frac{1+\nu}{1-\nu}\right]$$

where $\tau = \frac{\sigma_r - \sigma_\theta}{2}$

$$\tau = \frac{\sigma_r}{2}\left[\frac{1-2\nu}{1-\nu}\right]$$

Assumes τ relatively constant over

P_m of interest.

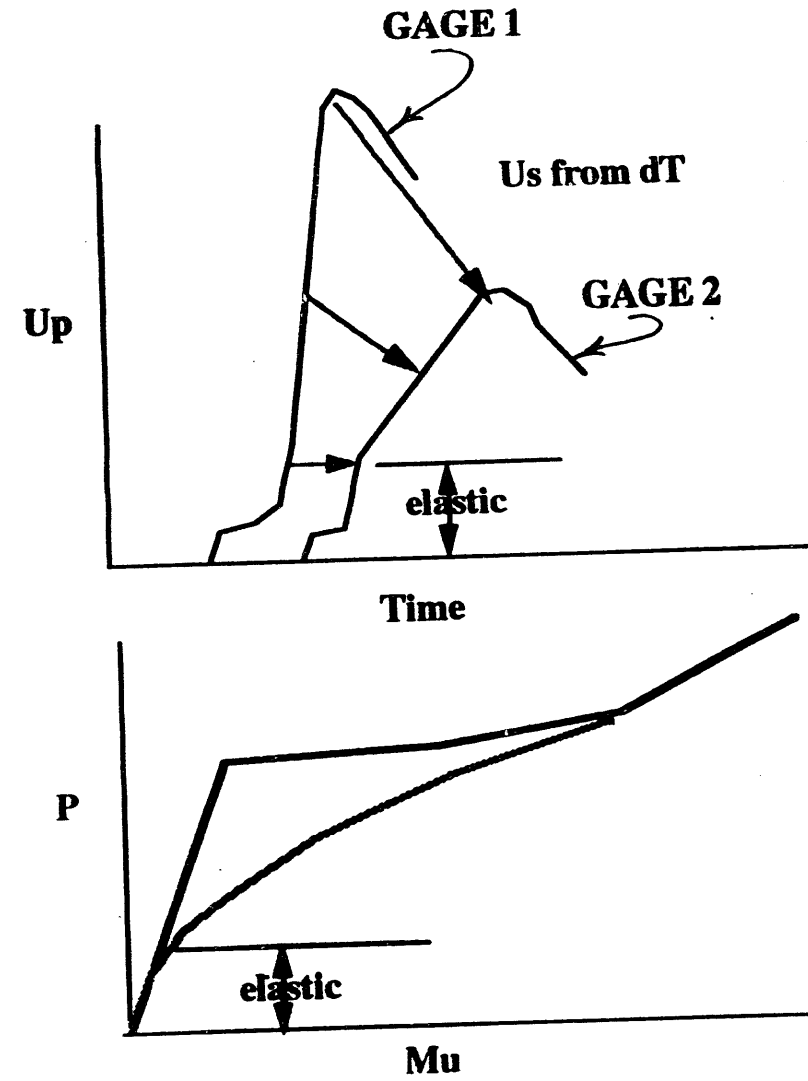

Figure 6. Method of establishing the elastic limit and shape of the P vs mu relationship.

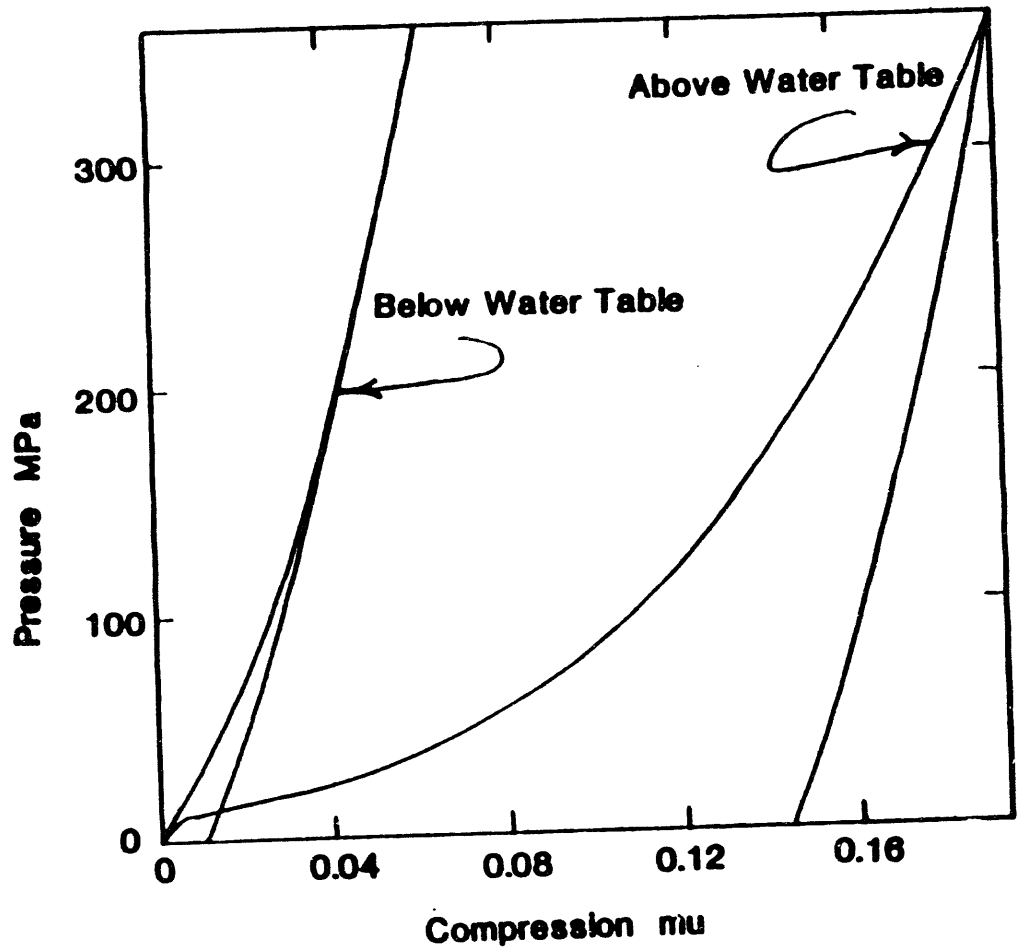

Figure 7. Comparison of the P vs mu relationships below and above the water table.

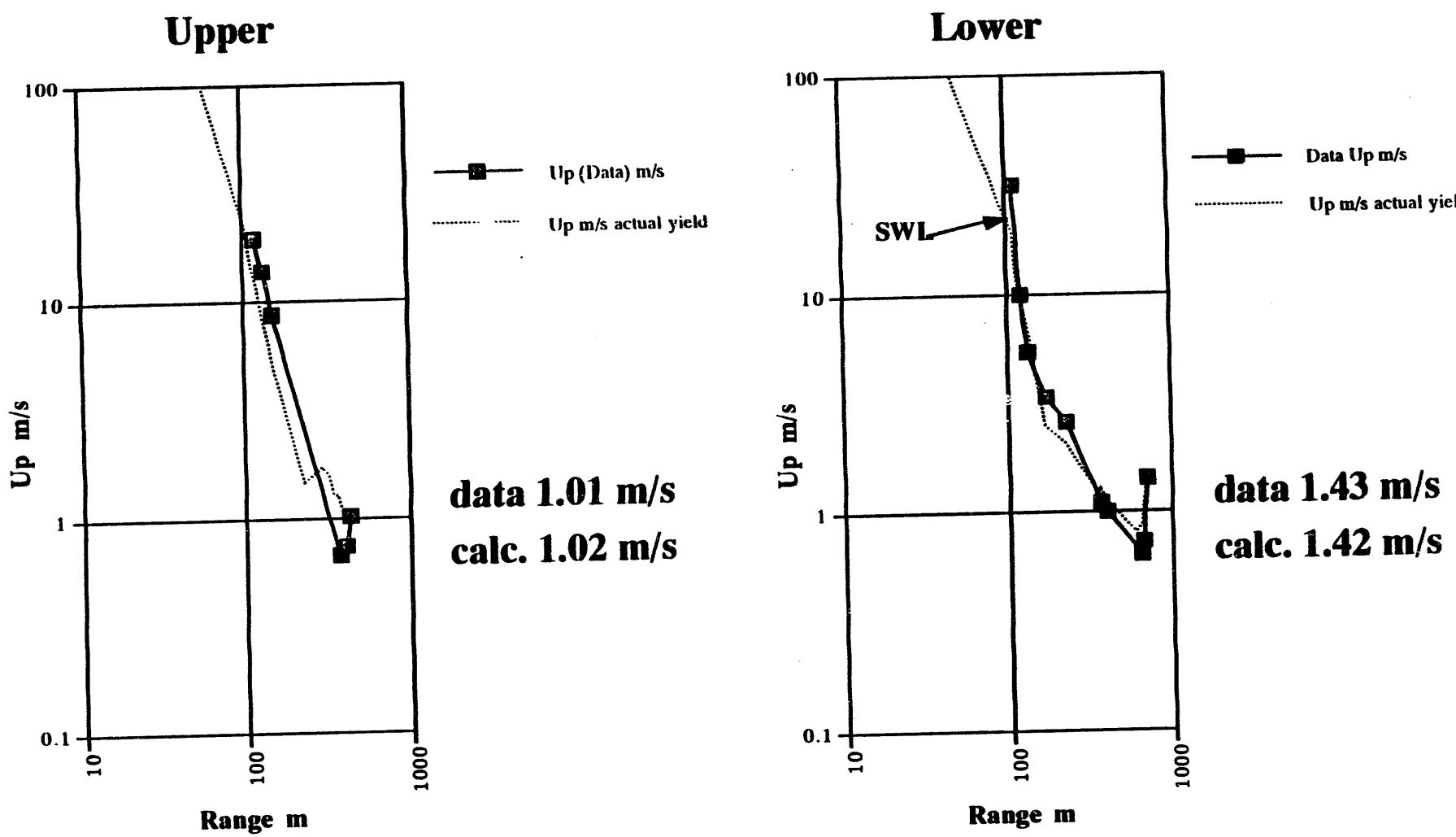

Figure 8. Free surface velocity has good agreement to modified-strength calculation run at actual yield. The upper event calculation shows poor agreement to the near surface data and the agreement at the surface may be fortuitous.

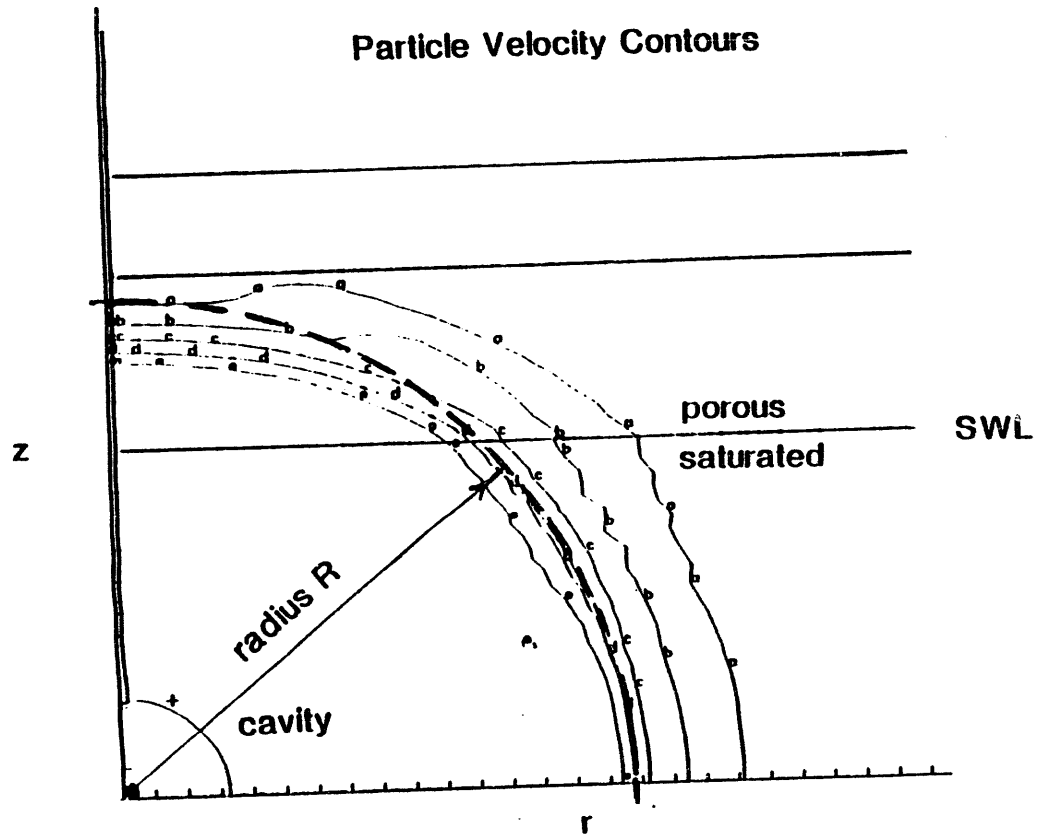

Figure 9. Flattening of the particle velocity wave above the water table is shown by comparison to a circular contour of radius R. Above the SWL the circular contour crosses over the velocity contours indicating a flatter wave front.

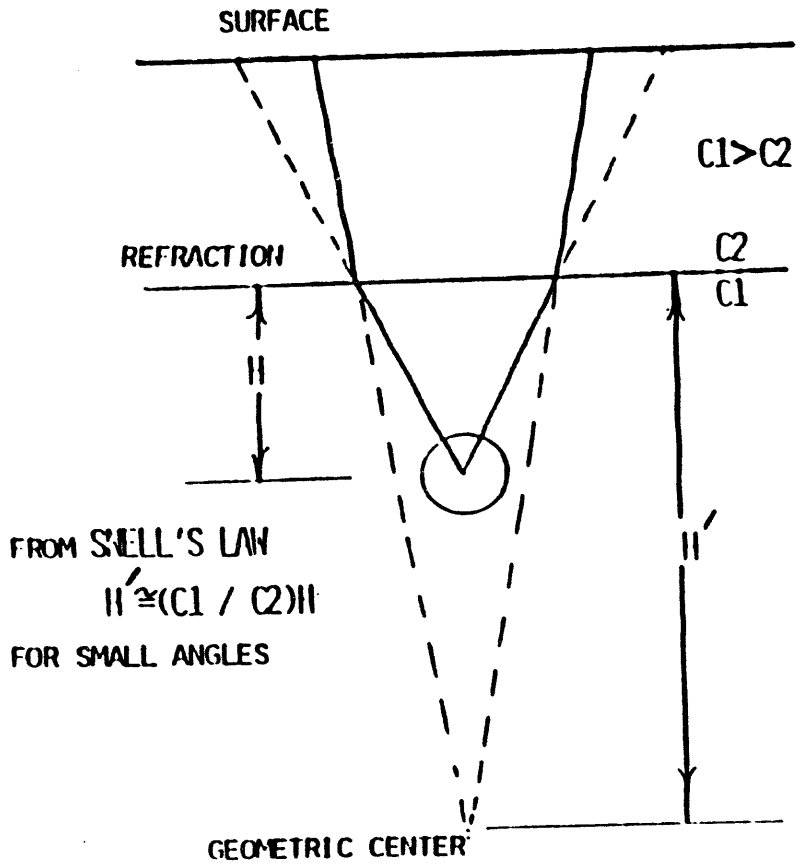

Figure 10 a. Schematic of Snell's law focussing. The solid line shows the change in radial divergence from the actual source center H below the SWL to an apparent source center H' above the SWL.

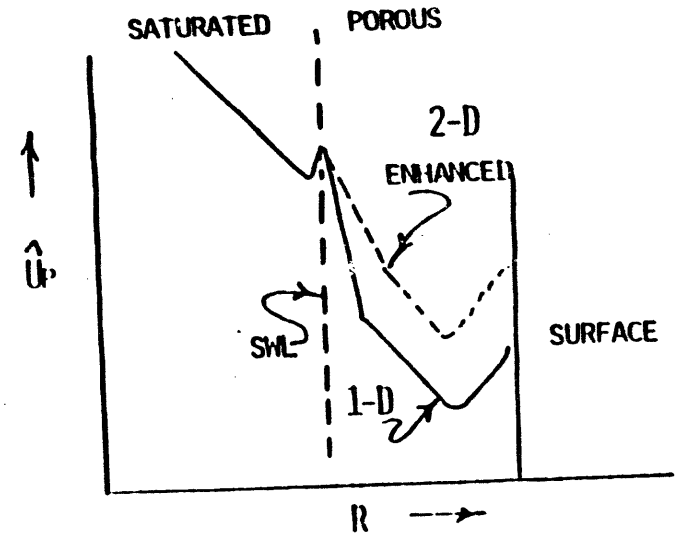

Figure 10 b. Schematic of attenuation difference between 1-D and 2-D calculations. Above the SWL the 2-D calculations show higher "enhanced" peak velocities due to the reduced radial divergence.

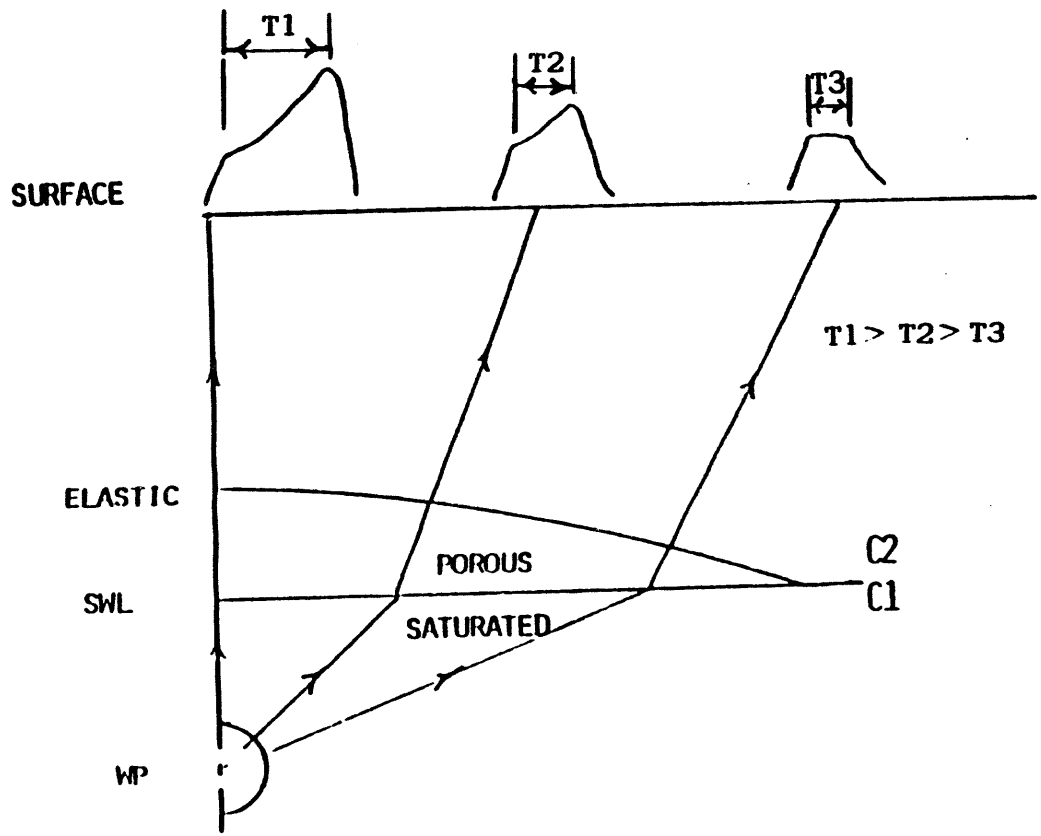

Figure 11. Schematic shows axial preference of porous crush and evidence found from surface velocity gages observed at he TYBO event. The peak of the wave travels slowly in the pore crush phase above the SWL and below the elastic curved line. Axially, the incident wave has the highest stress at the SWL than any other path. The axial stress takes longer and a greater distance for the peak to attenuate to elastic stress. Observations on TYBO showed wave forms along the surface which verified the diminishing time between elastic portions of the wave and the remnant of the plastic peak.

DATE
FILMED
8/17/94
END